Deep Learning methods evaluation to predict air quality based on computational fluid dynamics

Xavier Jurado, Nicolas Reiminger, Marouane Benmoussa, José Vazquez, Cédric Wemmert

Version of Record: https://www.sciencedirect.com/science/article/pii/S0957417422006595
Manuscript_cdf176d4a37f8c409a9eee51808e14da

Deep Learning methods evaluation to predict air quality based on computational fluid dynamics

Xavier Jurado[a,b,c] (xjurado@air-d.fr), Nicolas Reiminger[c] (nreiminger@air-d.fr), Marouane Benmoussa[c] (benmoussa.marouanee@gmail.com), José Vazquez[b] (jose.vazquez@engees.eu), Cédric Wemmert[c] (wemmert@unistra.fr)

[a] ICube Data mining: 300 Bd Sébastien Brant, Illkirch-Graffenstaden, France

[b] ICube Fluid mechanics: 2 Rue Boussingault, Strasbourg, France

[c] Air&D: 32 rue Whimpheling, Strasbourg, France

Corresponding Author:

Xavier Jurado

Air&D, 32 rue Whimpheling, F-67000 Strasbourg, France

Tel: +33 615 112 254

Email: xjurado@air-d.fr

Deep Learning methods evaluation to predict air quality based on computational fluid dynamics

Xavier Jurado[a,b,1,*], Nicolas Reiminger[c], Marouane Benmoussa[c], José Vazquez[b], Cédric Wemmert[a]

[a] *ICube Data mining: 300 Bd Sébastien Brant, Illkirch-Graffenstaden, France*
[b] *ICube Fluid mechanics: 2 Rue Boussingault, Strasbourg, France*
[c] *Air&D: 32 rue Whimpheling, Strasbourg, France*

Abstract

Air quality is a major health issue for densified cities nowadays. To evaluate and act upon it, modeling alongside sensors has proved to be a powerful tool. Among the different available models, Computational Fluid Dynamics (CFD) has proved to be formidable to evaluate airborne pollutant dispersion locally in urban areas since it is able to consider buildings and others complexes phenomenon at the scale of the meter. Nevertheless, this method has a major drawback, it is computationally expensive and cannot be applied in real time or over large areas. To overcome this issue, several state-of-the-art deep learning methods to treat spatial information have been trained based on CFD results to predict airborne pollutant dispersion. Among these models, multiResUnet architecture was proved to be the best on overall over seven metrics. It managed to have two out of three air quality metrics within acceptable range for a good air quality model. These results are obtained in a mere matter of minutes against several tenth of hours for CFD.

Keywords: Deep Learning, Convolutional Neural Network, Computational Fluid Dynamics, Air quality

*Corresponding author.
Email addresses: xjurado@air-d.fr (Xavier Jurado), nreiminger@air-d.fr (Nicolas Reiminger), benmoussa.marouanee@gmail.com (Marouane Benmoussa), jose.vazquez@engees.eu (José Vazquez), wemmert@unistra.fr (Cédric Wemmert)

1. Introduction

Atmospheric pollution represents millions of deaths each year and is one of the major health issues according to the World Health Organisation (WHO) since 91% of people lives in areas exceeding the WHO threshold standards (WHO, 2018). Indeed, airborne pollution can cause several mortal diseases (Yang et al., 2020; Calderón-Garcidueñas et al., 2020). It is also detrimental to the environment, causing acid rains (Zhang et al., 2017) or impacting agricultural yield (Wang et al., 2020). To tackle this issue, regulation has been implemented in Europe through the European Directive in 2008 (EU, 2008). The regulation is based on annual average as well as hourly concentrations that should not be exceeded. To ensure that these standards are respected and to protect health of residents, several tools exist to assess the pollution in an area. These tools can span continents (Blocken et al., 2015) to urban neighborhoods. For local pollution at the scale of the neighborhood, one can either use sensors (Jurado et al., 2020), but they are expensive and only provide very local information, or numerical models based on physical phenomena (Reiminger et al., 2020a). A popular approach for local pollution assessment is to simulate its dispersion with Computational Fluid Dynamics (CFD), but this requires a lot of computing resources (Jurado et al., 2021). It is therefore adapted to compute mean annual average but is not ideal for large areas or use in real time. On the other hand, to cover large areas in real time, some models like plume exist. Unfortunately, they are based on hypothesis that make them unsuited for urban areas where the air pollution is the most stringent (Kumar et al., 2015). The recent advances in machine learning and deep learning may provide the answer to these limitations. Indeed, it has much progressed over the recent years especially thanks to the improvement and democratisation of highly threaded parallel computing processors (Boyer & Baz, 2013). Recently, it has proved to outperform previous state of the art methods in various fields such as speech recognition, visual object recognition, object detection and many other domains such as drug discovery or genomics (LeCun et al., 2015). These new methods

have not gone unnoticed in the domain of physics and numerical simulation. Their use are still nascent in these domains. For example, deep learning models were trained to perform numerical simulation to accelerate them as in (Prieler et al., 2018; Guo et al., 2016; Junfeng Chen, 2019). Deep learning has also been used in the domain of air quality to estimate the pollution based on pictures (Chen et al., 2019), to predict the pike of pollution harmful to health (Morabito & Versaci, 2003), concentration values from sensors data (Du et al., 2021), to forecast air quality indicators (Kurt & Oktay, 2010; Yan et al., 2021), to extract the main features explaining the pollution variation (Qi et al., 2018). To build a fast and accurate system able to predict air pollution in real time based on wind, traffic and buildings geometry, we tried to use a convolutional network (CNN), that has proven to be able to treat spatial information successfully, to learn pollutant dispersion from CFD. This will overcome the issue of speed related to standard CFD computation while proposing a model that is more appropriate to urban areas. In this paper, 6 CNN models (namely UNet, SegNet, linkNet, MultiResUnet, PSPNet and FCN) are trained and tested, based on 5000 CFD examples. The aim of the paper is to verify the capability of such models to determine pollutant dispersion rapidly and accurately, and which of these well known CNN architecture performs better to solve this problem.

2. Material and methods

2.1. Physical numerical model

To learn pollutant dispersion in open urban areas, deep learning architectures need examples to be trained. To simulate wind and underlying pollutant dispersion, a popular technique is to use CFD as in (Murakami, 1998; Blocken, 2014; Reiminger et al., 2020a). To perform simulations, Openfoam 5.0 was used. OpenFoam[1] is an open source software dedicated to numerical simulations, ranging from financial to radiation to fluids mechanics. Hypothesis for the simulation were the following:

[1] `https://www.openfoam.org/`

– Reynolds Averaged Navier Stokes (RANS) approach was used;

– unsteady simulations were performed;

– the turbulence model for the RANS model is k-epsilon renormalization group (RNG) proposed by (Yakhot et al., 1992);

– a transport equation for the pollutant dispersion;

– upper and lateral boundaries are symmetry conditions;

– the outlet is a freestream condition;

– buildings have no slip conditions;

– the atmosphere is considered neutral, therefore using a logarithmic inlet profile and turbulence for k and epsilon parameter calculated as proposed in (Richards & Norris, 2011):

$$U = \frac{u_*}{\kappa_{k-\epsilon}} ln \frac{z_0 + z}{z_0} \tag{1}$$

$$\epsilon = \frac{u_*^2}{\sqrt{C_\mu}} \tag{2}$$

$$k = \frac{u_*^3}{\kappa_{k-\epsilon} z} \tag{3}$$

where, U is the inlet speed $[m.s^{-1}]$, ε is the turbulent dissipation rate $[kg.m^{-1}.s^{-4}]$, k is the turbulent kinetic energy $[kg.m^{-1}.s^{-3}]$, u_* is the shear velocity [m/s], $\kappa_{k-\epsilon}$ is the von Kármán constant, z_0 is the roughness length [m] and z is the altitude [m].

Guidelines provided by (Franke et al., 2007) were respected when constructing the domain and the meshes of every simulation. For each simulation, the top of the domain is situated at a minimum distance of $5 \times H$ from highest building and the lateral, inlet and outlet boundaries at a minimum distance of $5 \times H$ from the closest building, with H the height of the tallest building in

the domain. A mesh sensitivity analysis was made and a mesh with $0.5m$ for the cell closest to the building were found to be enough to be insensitive. An example of a neighborhood of the meshing is shown on Figure 1.

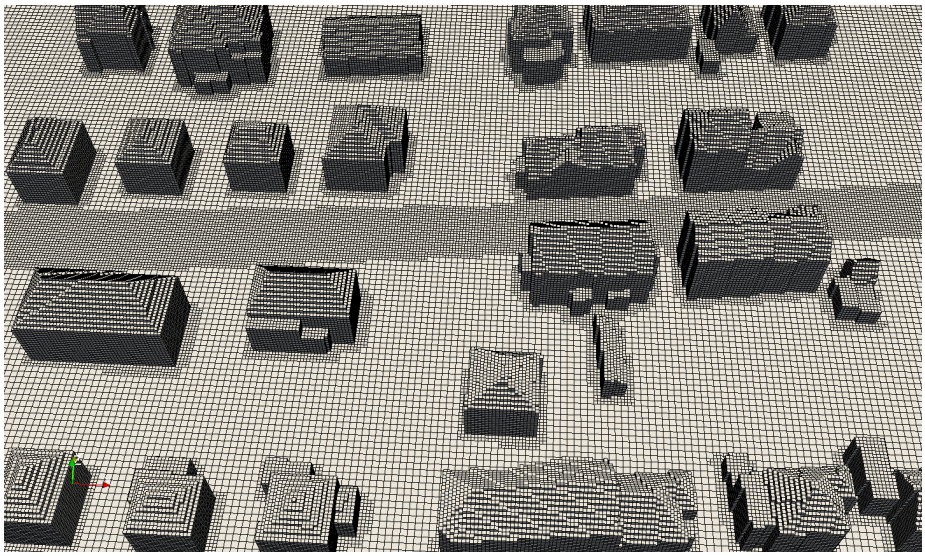

Figure 1: Example of the meshing on a building layout used to create the examples

More details on the model, equations and validation, please refer to (Reiminger et al., 2020b) where the same approach has been described and properly validated.

The approach, model and meshes described above have been found to be able to reach an error which is less than 10% compared to experimental measures as show in (Reiminger et al., 2020b) and a similar approach have been proven to have an overall error of about 30% compared to a real *in situ* situation in urban areas (Rivas et al., 2019). The numerical results will be considered as the ground truth for the deep learning algorithms.

For the sake of simplicity the wind will always come down from the y axis. Around $5,000$ examples of couples of building layouts and pollutant sources have been computed to be used for the deep learning training and validation.

2.2. Deep learning architectures

Deep learning architectures have shown to be very effective to tackle spatial information in various domain such as predicting urban traffic (Pan et al., 2020), (Tedjopurnomo et al., 2020) or to forecasting crop yield (Gavahi et al., 2021). Furthermore, convolutional ones have shown to be very effective. Indeed, for semantic segmentation, CNNs have proven to be able to overcome issues that were not achievable before in a lot of different fields. For example, it has been used in the medical field to identify certain cell types as in (Das & Meher, 2021), for small object detection (Liu et al., 2021), predict ozone concentration 24 hours in advance as in (Sayeed et al., 2020) or remote sensing images analysis (Wagner et al., 2020).

The strength of CNNs to treat spatial information have also started to be used to predict physical phenomena as in (Guo et al., 2016) and (Junfeng Chen, 2019). To simulate physical phenomena, such as fluid mechanics, it is common to define a set of fundamental equations describing the phenomena and then, if needed, to implement a numerical code that will solve them step by step, until reaching convergence (or pseudo convergence) or during the transient wanted time. These steps generally require vast computing time resources.

Deep learning has already been used in fluid mechanics, especially to determine the speed vector field (Guo et al., 2016; Junfeng Chen, 2019). Here, we have the ambition to go further and study the ability of such architectures to build a model able to determine pollution dispersion given buildings' geometry, wind and traffic information. For that, CNN's architectures designed for image segmentation tasks will be compared. The first architectures used are encoder-decoder, with, chronologically, Unet (Ronneberger et al., 2015), SegNet (Badrinarayanan et al., 2017), linkNet (Chaurasia & Culurciello, 2017) and multiResUnet (Ibtehaz & Rahman, 2020). They follow the same principle of encoding the information to get the context and then decoding it to get the precise location of the wanted feature. However they have small variants on the way they handle spatial information through the layers. A multi scale representation method with PSPNet (Zhao et al., 2017) will also be used. And finally,

a classical full convolutional network (FCN) (Long et al., 2015).

The models can have different number of free parameters depending on the number of layers and filters at each layer. To test different numbers of trainable parameters, the architectures will be tested with several filter per level. Each of this architectures have a level in which the number of filter is minimal as it can seen on 2 noted "F". This min filter will be used to describe the variation of free parameters in the models.

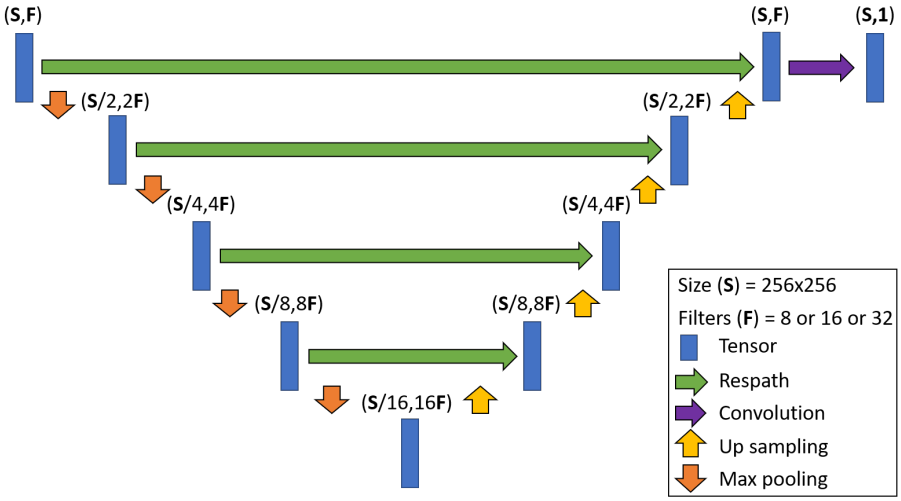

Figure 2: Architecture of the multiResUnet

2.3. Input and output data for the deep learning models

The computation from the physical model are turned into 2D maps of $150 \times 150m^2$ at a height of $1.5m$. Two maps will be used as input, the first map representing the height of the buildings and the second second map the distance from the pollutant source. The last map, will be the normalised pollutant dispersion field. An example of the images used the architectures are shown below:

In this study, $4,919$ examples were produced, divided with $3,687$ for training, 410 for validation and 822 divided into 28 subsets for testing according to the methodology provided by (Fawaz et al., 2019). The training was performed for

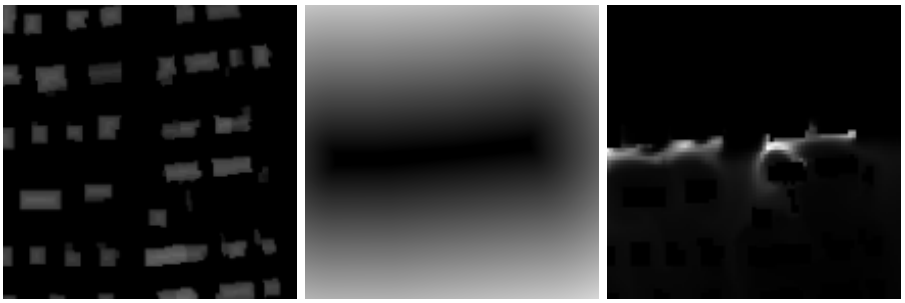

(a) Buildings (b) Pollution source (c) CFD result

Figure 3: Images given as input to the network (a) the height, shape and position of each building in the area, (b) the distance from the pollution source, and (c) the corresponding CFD simulation, considered as the right output for the CNN.

25 epochs with a batch size of 6. The optimizer used is Adam. A callback patience of 5 epochs was used on the validation data loss.

2.4. Deep learning loss

For every model, three losses are tested. Two well known losses, binary crossentropy (bce) and mean squared error (mse) as defined in Equations 4 and 5.

$$bce = \frac{1}{N}\sum_{i=1}^{N} y_i log(\hat{y_i}) + (1 - y_i) log(1 - \hat{y_i}), \tag{4}$$

$$mse = \frac{1}{N}\sum_{i=1}^{N} (y_i - \hat{y_i})^2 \tag{5}$$

A custom loss, called $J_{3D}loss$, was also tested (see Eq. 6). It is based on the Jaccard index, originally called community coefficient, that aims at comparing the intersection with the union of two binary set. This index is often used in segmentation to compare the predicted binary mask to a ground truth segmentation mask. But here, the pollutant concentration is a continuous value, so areas can not be compared as in segmentation. However, the continuous value can be considered as a third dimension and so the intersection over the union is not computed between two surfaces but two volumes. The loss is computed between two pairs of images as following:

$$J_{3D}\ loss = 1 - \frac{V_{pred} \bigcap V_{true}}{V_{pred} \bigcup V_{true}} \simeq 1 - \frac{1}{N} \sum_{i=1}^{N} \frac{min(y_i, \hat{y_i})}{max(y_i, \hat{y_i})} \tag{6}$$

where V_{pred} and V_{true} are the respective volume of the two images with the pixel value as the thir dimension respectively for the predicted and ground truth image, N is the number of pixels, yi_i^{true} is the value of the i^{th} pixel of the true image and yi_i^{true} is the value of the i^{th} pixel in the predicted image.

Models	**Min filters**	**Losses**
FCN	1 - 2 - 4 - 8	J_{3D} - bce - mse
PSPNet	8 - 16	J_{3D} - bce - mse
linkNet	8 - 16 - 32	J_{3D} - bce - mse
SegNet	8 - 16 - 32	J_{3D} - bce - mse
multiResUnet	8 - 16 - 32	J_{3D} - bce - mse
Unet	8 - 16 - 32	J_{3D} - bce - mse

Table 1: Summary of the different variants of each model tested in this study

2.5. Evaluation of the results

2.5.1. Popular metrics in the air quality field

To evaluate the predictions made by the deep learning architectures, several metrics will be used. Indeed, each measures different aspects of the model and helps to see strength and weaknesses better than reducing the analysis on one single metric. In the air quality field, the study of Chang *et al.* (Chang & Hanna, 2004) provides several metrics to be used to evaluate and conclude on the quality of a model. Six metrics are provided, but some are equivalent and evaluate the same aspect of the result. Thus, we keep only four of them for the presented study. Fractional Bias (FB) measures if the prediction mean is globally the same as the ground truth mean value. Normalised Mean Squared Error ($NMSE$) measures if there are extreme differences between the prediction and the ground truth. The fraction of predictions within a factor of two of observations ($FAC2$) enables to measure that on overall, the predictions are within an accepting error margin. And finally, R index, that compares the

correlation between the two datasets (ground truth and predictions). FB and $NMSE$ are to be minimized at 0, $FAC2$ and R are to be maximized at 1.

$$FB = \frac{(\overline{C_{ref}} - \overline{C_{pred}})}{0.5(\overline{C_{pred}} + \overline{C_{ref}})}, \tag{7}$$

$$NMSE = \frac{\overline{(C_{ref} - C_{pred})^2}}{C_{pred} C_{ref}}, \tag{8}$$

$$FAC2 = \text{fraction of data that satisfy } 0.5 < \frac{C_{pred}}{C_{ref}} < 2, \tag{9}$$

$$R = \frac{\overline{(C_{ref} - \overline{C_{ref}})(C_{pred} - \overline{C_{pred}})}}{\sigma_{C_{pred}} \sigma_{C_{ref}}}, \tag{10}$$

with C_{pred} the predicted concentration field and C_{ref} the reference concentration field (ground truth).

In (Chang & Hanna, 2004), the authors propose ranges of values on the above parameters to assess if an air quality model is satisfying. They also underline that for spatial models, these values are harder to reach. The proposed values are:

- FAC2 > 0.5,
- NSME < 1.5,
- $|\text{FB}| < 0.3$.

2.5.2. Metrics related to images

On the above metrics, three more that are commonly used to compare images will be estimated. The relative mean absolute error (MAE_{rel}), J_{3D} that is also used as a loss and described previously, and the Structural Similarity Index ($SSIM$) designed to measure the visual quality between a compressed image and the original one. MAE_{rel} is to be minimized. $SSIM$ and J_{3D} are to be maximized.

$$MAE_{rel} = \frac{|C_{ref} - C_{pred}|}{\overline{C_{pred}}} \tag{11}$$

$$J_{3D} \simeq \frac{min(C_{ref}, C_{pred})}{max(C_{ref}, C_{pred})} \tag{12}$$

with C_{pred} the model prediction concentration and C_{ref} the reference concentration (ground truth).

$$SSIM(A, B) = \frac{(2\mu_A\mu_B + c_1)(2\sigma_{AB} + c2)}{(\mu_A^2 + \mu_B^2 + c1)(\sigma_A^2 + \sigma_B^2 + c2)} \tag{13}$$

$$c_1 = (k_1 L)^2 \quad c_2 = (k_2 L)^2 \tag{14}$$

where μ_A and μ_B are the respective average of A and B, σ_A^2 and σ_B^2 are the respective variances of A and B, σ_{AB} is the covariance of A and B, L is the dynamic range of the pixel values and k_1 and k_2 are two constants respectively 0.01 and 0.03 (by default).

3. Results

To compare the architectures, the methodology provided in (Fawaz et al., 2019) will be used. This methodology allows to compare different models by ranking them on their performance on a metric over several datasets. This ranking can then be used to make a critical difference diagrams. To compare the models, the test dataset composed of 822 examples divided into 28 subdatasets will be used. A subdataset correspond to an emission source (road) with a building outlet.

3.1. Loss functions and filters

Three loss functions were tested along several number of filters for each 6 model. The difference between predictions and ground truth was evaluated according the 7 metrics presented above. Nevertheless, as this would produce $7 \times 6 = 49$ diagrams, to sum up the result, the 7 metrics of each variant were concatenated together for each model to determine the best performing variant for each model. Thus, the 6 models diagrams are presented on the critical difference diagrams in Figure 4. Notations on the diagram for the model are

"loss"_"min filters", for example a model that uses binary crossentropy and 4 min filters will be noted "bce_4".

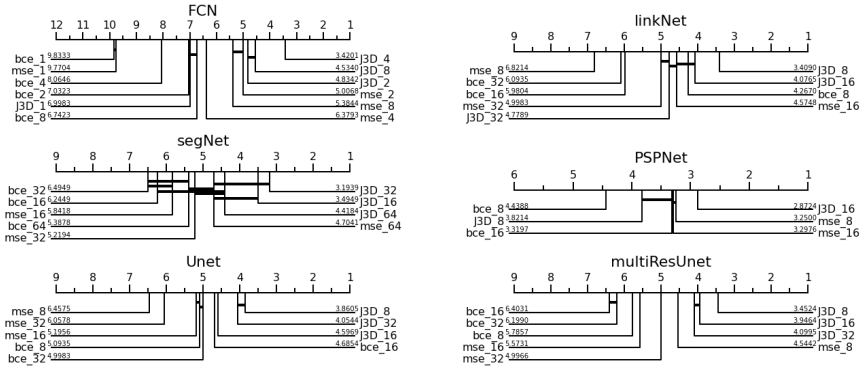

Figure 4: Ranking of the different variants for each model using all the metrics

As it can be seen on Figure 4, the J_{3D} loss always comes first for every model.

3.2. Architectures

Using the best variant of each model as determined in the previous subsection. The same approach of the critical difference diagram will be used to determine which model performs best. The results for all the metrics with all the best variant of each model is presented on the Figure 5

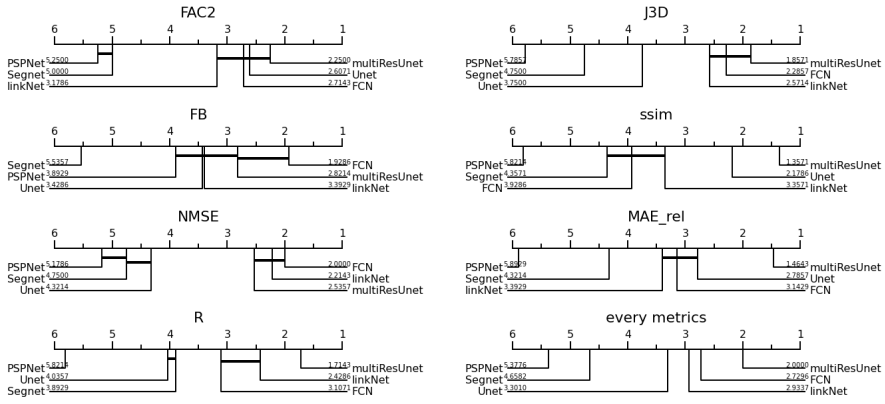

Figure 5: Ranking of each best variant for each model according to each metric

metric	**FAC2**	**NMSE**	**FB**	**R**	**MAE rel**	**J3D**	**ssim**
mean value	0.8	3.7	0.3	0.8	0.7	0.5	0.8
expected value	$\approx > 0.5$	$\approx < 1.5$	$\approx < 0.3$	1	0	1	1

Table 2: Evaluation of the results of the multiResUnet on each metric

The architecture that manages to predict best pollutant dispersion on overall is multiResUnet which is first 5/7 times and always at least in the first statistically indistinguishable group. When all metrics are considered together, multiResUnet becomes first. The absolute results on all metrics for multiResUnet using 8 min filters and J_{3D} are given in Table 2. It can be seen that multiResUnet using the J_{3D} loss managed to perform within the standard performance of a good model for 2 out of 3 metrics widely used in air quality.

Examples of the multiResUnet predictions against the CFD model for the centile 5 %, the median and the centile 95 % of J_{3D} are shown on Figure 6.

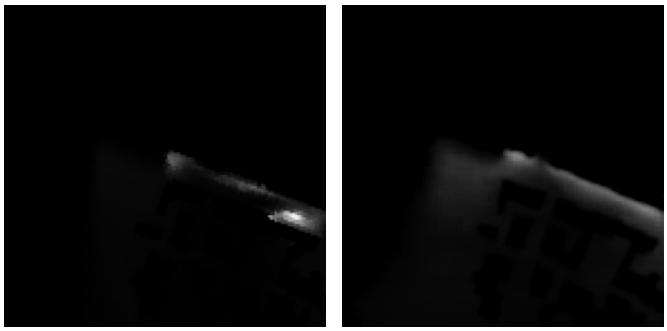

(a) ground truth

(b) prediction $J_{3D} = 0.32$ (Centile 5%)

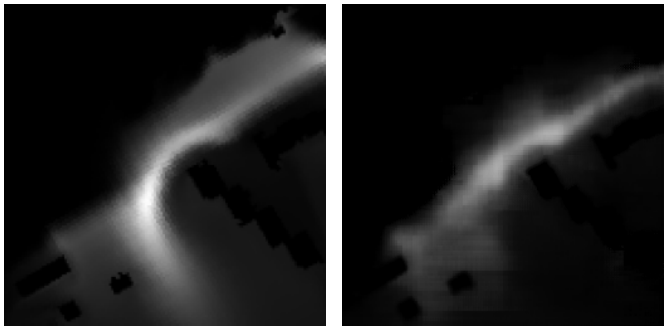

(c) ground truth

(d) prediction $J_{3D} = 0.49$ (Median)

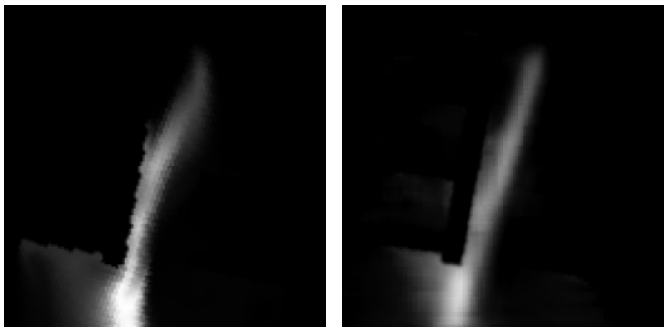

(e) ground truth

(f) prediction $J_{3D} = 0.63$ (Centile 95%)

Figure 6: Examples of predictions from the multiResUnet

4. Conclusion

Several architectures that have proved their efficiency in other field have been applied to pollutant dispersion modeling. For each of these architectures, several variants with different amount of minimal filters were trained using three different losses. For each model, the variants were compared against several metrics and it was found that J_{3D} loss gave the best results for every model to predict airborne pollutant dispersion. The architectures were then compared one against the others and it was found that multiResUnet had the overall best results. Using metrics wildly accepted in the air quality field, 2 out of the 3 metrics are in the accepted range for a good air quality model when compared to the ground truth. The architecture was able to obtain these results in minutes compared to the computation that requires tenths of hours. These results are promising to enable real time pollutant dispersion in urban cities with CFD accuracy. Indeed, this Deep Learning model could be the milestone of an intelligent system to assess air pollution from traffic in real time.

5. Acknowledgments

The authors would like to thank Nvidia for providing a free Titan V GPU through their academic grant. The authors would like to thank the *Association Nationale de la Recherche et de la Technologie* (ANRt) for supporting the PhD.

References

Badrinarayanan, V., Kendall, A., & Cipolla, R. (2017). SegNet: A deep convolutional encoder-decoder architecture for image segmentation. *IEEE Transactions on Pattern Analysis and Machine Intelligence*, *39*, 2481–2495. doi:10.1109/tpami.2016.2644615.

Blocken, B. (2014). 50 years of Computational Wind Engineering: Past, present and future. *Journal of Wind Engineering and Industrial Aerodynamics*, *129*, 69–102. doi:10.1016/j.jweia.2014.03.008.

Blocken, B., van der Hout, A., Dekker, J., & Weiler, O. (2015). CFD simulation of wind flow over natural complex terrain: Case study with validation by field measurements for Ria de Ferrol, Galicia, Spain. *Journal of Wind Engineering and Industrial Aerodynamics*, *147*, 43–57. doi:10.1016/j.jweia.2015.09.007.

Boyer, V., & Baz, D. E. (2013). Recent advances on GPU computing in operations research. In *2013 IEEE International Symposium on Parallel & Distributed Processing, Workshops and Phd Forum*. IEEE. doi:10.1109/ipdpsw.2013.45.

Calderón-Garcidueñas, L., Herrera-Soto, A., Jury, N., Maher, B. A., González-Maciel, A., Reynoso-Robles, R., Ruiz-Rudolph, P., van Zundert, B., & Varela-Nallar, L. (2020). Reduced repressive epigenetic marks, increased DNA damage and Alzheimer's disease hallmarks in the brain of humans and mice exposed to particulate urban air pollution. *Environmental Research*, *183*, 109226. doi:10.1016/j.envres.2020.109226.

Chang, J. C., & Hanna, S. R. (2004). Air quality model performance evaluation. *Meteorology and Atmospheric Physics*, *87*. doi:10.1007/s00703-003-0070-7.

Chaurasia, A., & Culurciello, E. (2017). LinkNet: Exploiting encoder representations for efficient semantic segmentation. In *2017 IEEE Visual Communications and Image Processing (VCIP)*. IEEE. doi:10.1109/vcip.2017.8305148.

Chen, L., Ding, Y., Lyu, D., Liu, X., & Long, H. (2019). Deep Multi-Task Learning Based Urban Air Quality Index Modelling. *Proceedings of the ACM on Interactive, Mobile, Wearable and Ubiquitous Technologies*, *3*, 1–17. doi:10.1145/3314389.

Das, P. K., & Meher, S. (2021). An efficient deep convolutional neural network based detection and classification of acute lymphoblastic leukemia. *Expert*

Systems with Applications, *183*, 115311. URL: https://doi.org/10.1016/j.eswa.2021.115311. doi:10.1016/j.eswa.2021.115311.

Du, S., Li, T., Yang, Y., & Horng, S. (2021). Deep air quality forecasting using hybrid deep learning framework. *IEEE Transactions on Knowledge & Data Engineering*, *33*, 2412–2424. doi:10.1109/TKDE.2019.2954510.

EU (2008). *Directive 2008/50/EC of the european parliament and of the council of 21 May 2008 on ambient air quality and cleaner air for Europe*. European Union.

Fawaz, H. I., Forestier, G., Weber, J., Idoumghar, L., & Muller, P.-A. (2019). Deep learning for time series classification: a review. *Data Mining and Knowledge Discovery*, *33*, 917–963. doi:10.1007/s10618-019-00619-1.

Franke, J., Hellsten, A., Schlünzen, H., & Carissimo, B. (2007). Best practice guideline for the CFD simulation of flows in the urban environment. *COST Action 732*, .

Gavahi, K., Abbaszadeh, P., & Moradkhani, H. (2021). DeepYield: A combined convolutional neural network with long short-term memory for crop yield forecasting. *Expert Systems with Applications*, *184*, 115511. URL: https://doi.org/10.1016/j.eswa.2021.115511. doi:10.1016/j.eswa.2021.115511.

Guo, X., Li, W., & Iorio, F. (2016). Convolutional neural networks for steady flow approximation. In *Proceedings of the 22nd ACM SIGKDD International Conference on Knowledge Discovery and Data Mining*. ACM. doi:10.1145/2939672.2939738.

Ibtehaz, N., & Rahman, M. S. (2020). MultiResUNet : Rethinking the U-Net Architecture for Multimodal Biomedical Image Segmentation. *Neural Networks*, *121*, 74–87. doi:10.1016/j.neunet.2019.08.025. ArXiv: 1902.04049.

Junfeng Chen, E. H., Jonathan Viquerat (2019). U-net architectures for fast prediction in fluidmechanics. *hal-02401465*, .

Jurado, X., Reiminger, N., Vazquez, J., & Wemmert, C. (2021). On the minimal wind directions required to assess mean annual air pollution concentration based on CFD results. *Sustainable Cities and Society*, *71*, 102920. doi:10.1016/j.scs.2021.102920.

Jurado, X., Reiminger, N., Vazquez, J., Wemmert, C., Dufresne, M., Blond, N., & Wertel, J. (2020). Assessment of mean annual NO2 concentration based on a partial dataset. *Atmospheric Environment*, *221*, 117087. doi:10.1016/j.atmosenv.2019.117087.

Kumar, P., Feiz, A.-A., Ngae, P., Singh, S. K., & Issartel, J.-P. (2015). CFD simulation of short-range plume dispersion from a point release in an urban like environment. *Atmospheric Environment*, *122*, 645–656. doi:10.1016/j.atmosenv.2015.10.027.

Kurt, A., & Oktay, A. B. (2010). Forecasting air pollutant indicator levels with geographic models 3days in advance using neural networks. *Expert Systems with Applications*, *37*, 7986–7992. URL: https://doi.org/10.1016/j.eswa.2010.05.093. doi:10.1016/j.eswa.2010.05.093.

LeCun, Y., Bengio, Y., & Hinton, G. (2015). Deep learning. *Nature*, *521*, 436–444. doi:10.1038/nature14539.

Liu, Y., Sun, P., Wergeles, N., & Shang, Y. (2021). A survey and performance evaluation of deep learning methods for small object detection. *Expert Systems with Applications*, *172*, 114602. URL: https://doi.org/10.1016/j.eswa.2021.114602. doi:10.1016/j.eswa.2021.114602.

Long, J., Shelhamer, E., & Darrell, T. (2015). Fully convolutional networks for semantic segmentation. In *2015 IEEE Conference on Computer Vision and Pattern Recognition (CVPR)*. IEEE. doi:10.1109/cvpr.2015.7298965.

Morabito, F. C., & Versaci, M. (2003). Fuzzy neural identification and forecasting techniques to process experimental urban air pollution data. *Neural*

Networks, *16*, 493–506. URL: https://doi.org/10.1016/s0893-6080(03)00019-4. doi:10.1016/s0893-6080(03)00019-4.

Murakami, S. (1998). Overview of turbulence models applied in CWE–1997. *Journal of Wind Engineering and Industrial Aerodynamics*, *74-76*, 1–24. doi:10.1016/s0167-6105(98)00004-x.

Pan, Z., Zhang, W., Liang, Y., Zhang, W., Yu, Y., Zhang, J., & Zheng, Y. (2020). Spatio-temporal meta learning for urban traffic prediction. *IEEE Transactions on Knowledge and Data Engineering*, (pp. 1–1). doi:10.1109/tkde.2020.2995855.

Prieler, R., Mayrhofer, M., Gaber, C., Gerhardter, H., Schluckner, C., Landfahrer, M., Eichhorn-Gruber, M., Schwabegger, G., & Hochenauer, C. (2018). CFD-based optimization of a transient heating process in a natural gas fired furnace using neural networks and genetic algorithms. *Applied Thermal Engineering*, *138*, 217–234. doi:10.1016/j.applthermaleng.2018.03.042.

Qi, Z., Wang, T., Song, G., Hu, W., Li, X., & Zhang, Z. (2018). Deep air learning: Interpolation, prediction, and feature analysis of fine-grained air quality. *IEEE Transactions on Knowledge and Data Engineering*, *30*, 2285–2297. doi:10.1109/tkde.2018.2823740.

Reiminger, N., Vazquez, J., Blond, N., Dufresne, M., & Wertel, J. (2020a). CFD evaluation of mean pollutant concentration variations in step-down street canyons. *Journal of Wind Engineering and Industrial Aerodynamics*, *196*, 104032. doi:10.1016/j.jweia.2019.104032.

Reiminger, N., Vazquez, J., Blond, N., Dufresne, M., & Wertel, J. (2020b). CFD evaluation of mean pollutant concentration variations in step-down street canyons. *Journal of Wind Engineering and Industrial Aerodynamics*, *196*, 104032. doi:10.1016/j.jweia.2019.104032.

Richards, P., & Norris, S. (2011). Appropriate boundary conditions for com-

putational wind engineering models revisited. *Journal of Wind Engineering and Industrial Aerodynamics*, *99*, 257–266.

Rivas, E., Santiago, J. L., Lechón, Y., Martín, F., Ariño, A., Pons, J. J., & Santamaría, J. M. (2019). CFD modelling of air quality in Pamplona City (Spain): Assessment, stations spatial representativeness and health impacts valuation. *Science of the Total Environment*, (p. 19).

Ronneberger, O., Fischer, P., & Brox, T. (2015). U-net: Convolutional networks for biomedical image segmentation. In *International Conference on Medical image computing and computer-assisted intervention* (pp. 234–241). Springer.

Sayeed, A., Choi, Y., Eslami, E., Lops, Y., Roy, A., & Jung, J. (2020). Using a deep convolutional neural network to predict 2017 ozone concentrations, 24 hours in advance. *Neural Networks*, *121*, 396–408. URL: `https://doi.org/10.1016/j.neunet.2019.09.033`. doi:`10.1016/j.neunet.2019.09.033`.

Tedjopurnomo, D. A., Bao, Z., Zheng, B., Choudhury, F., & Qin, A. K. (2020). A survey on modern deep neural network for traffic prediction: Trends, methods and challenges. *IEEE Transactions on Knowledge and Data Engineering*, (pp. 1–1). doi:`10.1109/tkde.2020.3001195`.

Wagner, F. H., Dalagnol, R., Tarabalka, Y., Segantine, T. Y. F., Thomé, R., & Hirye, M. C. M. (2020). U-net-id, an instance segmentation model for building extraction from satellite images—case study in the joanópolis city, brazil. *Remote Sensing*, *12*. doi:`10.3390/rs12101544`.

Wang, Z., Wei, W., & Zheng, F. (2020). Effects of industrial air pollution on the technical efficiency of agricultural production: Evidence from China. *Environmental Impact Assessment Review*, *83*, 106407. doi:`10.1016/j.eiar.2020.106407`.

WHO (2018). *Burden of disease from ambient air pollution for 2016*. World Health Organization 2018.

Yakhot, V., Orszag, S. A., Thangam, S., Gatski, T. B., & Speziale, C. G. (1992). Development of turbulence models for shear flows by a double expansion technique. *Physics of Fluids A: Fluid Dynamics*, *4*, 1510–1520. doi:10.1063/1.858424.

Yan, R., Liao, J., Yang, J., Sun, W., Nong, M., & Li, F. (2021). Multi-hour and multi-site air quality index forecasting in beijing using CNN, LSTM, CNN-LSTM, and spatiotemporal clustering. *Expert Systems with Applications*, *169*, 114513. URL: https://doi.org/10.1016/j.eswa.2020.114513. doi:10.1016/j.eswa.2020.114513.

Yang, Z., Hao, J., Huang, S., Yang, W., Zhu, Z., Tian, L., Lu, Y., Xiang, H., & Liu, S. (2020). Acute effects of air pollution on the incidence of hand, foot, and mouth disease in Wuhan, China. *Atmospheric Environment*, *225*, 117358. doi:10.1016/j.atmosenv.2020.117358.

Zhang, G., Liu, D., He, X., Yu, D., & Pu, M. (2017). Acid rain in Jiangsu province, eastern China: Tempo-spatial variations features and analysis. *Atmospheric Pollution Research*, *8*, 1031–1043. doi:10.1016/j.apr.2017.02.001.

Zhao, H., Shi, J., Qi, X., Wang, X., & Jia, J. (2017). Pyramid scene parsing network. In *2017 IEEE Conference on Computer Vision and Pattern Recognition (CVPR)*. IEEE. doi:10.1109/cvpr.2017.660.